Cascaded optical parametric generation in reverse-proton-exchange lithium niobate waveguides

Xiuping Xie and M. M. Fejer

Edward L. Ginzton Laboratory, Stanford University, Stanford, California 94305, USA

Received May 4, 2006; revised August 28, 2006; accepted September 1, 2006;
posted October 11, 2006 (Doc. ID 69695); published February 15, 2007

Cascaded optical parametric generation in lithium niobate waveguides involves simultaneous quasi-phase-matching of optical parametric generation and sum-frequency generation. We study details of this process in reverse-proton-exchange lithium niobate waveguides with quasi-phase-matching gratings from 6 to 42 mm in length. We identify the cascaded products in the time domain using a frequency-resolved cross correlator and study cascaded optical parametric generation under different levels of pump depletion. With phase-modulated gratings, we demonstrate control over the wavelength of the near-transform-limited signal pulses from cascaded optical parametric generation. With its low threshold and controllable temporal properties, cascaded optical parametric generation in reverse-proton-exchange waveguides can be a promising candidate for a tunable light source.

OCIS codes: 190.4410, 190.7110.

1. INTRODUCTION

Optical parametric generation is the simplest in the family of parametric frequency converters, which are common sources for tunable ultrashort near-infrared and mid-infrared pulses. However, applications of optical parametric generation (OPG) are limited by its high threshold[1] and the often poor temporal properties of generated pulses. Recently we reported picojoule-threshold OPG in reverse-proton-exchange congruent lithium niobate waveguides with picosecond pump pulses near 780 nm, and near-transform-limited output obtained from cascaded OPG.[2] However, a systematic study of cascaded OPG was absent, and the simultaneous phase matching of OPG and sum-frequency generation (SFG) in uniform gratings was coincidental and hence not readily engineerable. In this paper, we analyze the details of cascaded OPG by studying it in uniform quasi-phase-matching (QPM) gratings of different lengths. Using a frequency-resolved cross correlator,[3] we directly identified the products from cascaded OPG and conventional OPG in the time domain using a single device at a fixed pump power. We also studied cascaded OPG under different levels of pump depletion. In addition, by phase modulating QPM gratings to synthesize desirable frequency responses, we were able to control the wavelength of the near-transform-limited signal from cascaded OPG. We may therefore widely tune the signal wavelength by switching between different devices on the same chip and temperature tune over a narrower wavelength range while retaining controlled temporal properties.

2. CONVENTIONAL OPTICAL PARAMETRIC GENERATION AND CASCADED OPTICAL PARAMETRIC GENERATION

Conventional OPG involves only three waves, the pump, the signal, and the idler. The pump photons split into signal and idler photons when energy conservation and phase-matching conditions are satisfied (in this paper, we define the signal and the idler as the shorter and longer output wavelengths, respectively). The bandwidth of the output pulses in conventional OPG usually is much broader than the transform limit, except for special combinations of pump, signal, and idler wavelengths.[4] In general, one can improve the temporal properties of the signal and idler by adding extra frequency filters at the expense of added complexity and significant energy loss. However, this high-energy loss can be avoided in cascaded OPG, which uses an extra parametric nonlinear process as the filter.

In contrast to conventional OPG, cascaded OPG involves four waves and only can occur at signal wavelengths where OPG and another parametric process are simultaneously phase matched. Figure 1 shows the constraints for cascaded OPG where the extra process is the SFG between the pump and the signal. Besides OPG and SFG, backconversion of the sum-frequency (SF) wave to the pump and signal waves is also necessary to obtain cascaded OPG. The phase-matching conditions of these processes can be simultaneously satisfied in QPM gratings by using different orders of QPM peaks or by engineering multicomponent QPM gratings.

0740-3224/07/030585-7/$15.00

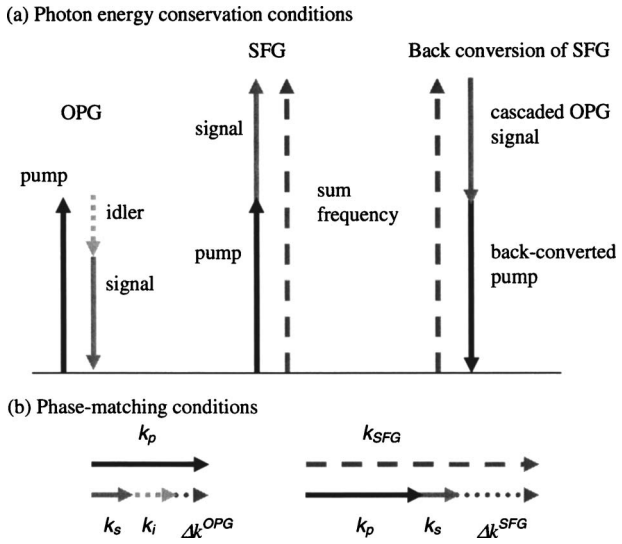

Fig. 1. Diagram of the constraints for cascaded OPG involving simultaneous QPM of OPG and SFG between the pump and the signal. k_p, k_s, k_i, and k_{SFG} are the wavenumbers of the pump, signal, idler, and the SF waves. $\Delta k^{OPG}(\Delta k^{SFG})$ is the wave-vector mismatch in the OPG (SFG) process. We may engineer QPM gratings to simultaneously satisfy both phase-matching conditions. (a) Photon energy conservation conditions, (b) phase-matching conditions.

We simulated cascaded OPG by solving the coupled evolution equations for the four waves involved [Eq. (1) in Ref. 2]. When the group velocity of both the signal and idler waves is faster than the pump wave while the extra wave at the sum frequency is slower than the pump wave, simulations and experimental results show that the temporal properties of the cascaded OPG products could be better controlled than those of the conventional OPG products.[2]

Although this extra phase-matched process improved the temporal properties of the output, it limited the tuning ability of the device. In the experiment described in Ref. 2, the signal and idler wavelengths from conventional OPG were tunable from 1.1 to 2.3 μm by tuning the pump wavelength from 770 to 790 nm.[2] However, in uniform QPM gratings, the center wavelength of the signal from cascaded OPG was not a strong function of the pump wavelength or the temperature. It could only be tuned by several nanometers at approximately three wavelengths: 1190, 1280, or 1430 nm. These three wavelengths correspond to the three strongest cascaded processes; other cascaded processes are insignificant. Besides involving optical parametric generation with first-order QPM, these three cascaded processes, respectively, involve second-harmonic generation of the signal, which generates yellow light at ~595 nm with second-order QPM, SFG between the pump and the idler, which generates green light at ~550 nm with second-order QPM, and SFG between the pump and the signal, which is illustrated in Fig. 1 and generates green light at ~500 nm with third-order QPM. Without losing generality, in this paper, we only consider the last two strong cascaded OPG processes involving SFG.

In the following sections, we present experimental results for cascaded OPG in uniform gratings of various lengths and in engineered QPM gratings. We demonstrate that the temporal properties of the OPG products can be controlled using cascaded OPG and synthesized QPM gratings.

3. EXPERIMENTS WITH UNIFORM QUASI-PHASE-MATCHING GRATINGS

In Ref. 2 we demonstrated that the conventional OPG and cascaded OPG products were distinguishable both in the time domain and in the frequency domain by studying the output from the same uniform QPM grating at various pump power levels. When the QPM grating length was long enough and the pump power was high enough, cascaded OPG appeared as new peaks in both domains. In the present study, described in this section, we study cascaded OPG more systematically by testing uniform QPM gratings of different lengths and analyzing the properties of OPG products using frequency-resolved cross correlation.[3] At the end of this section, we compare the signal and idler pulse shapes.

In the experiments reported here, the FWHM duration of the pump pulses was 1.8 ps, all the interacting waves were in the TM_{00} waveguide mode, the QPM grating periods in the devices were 16.45 μm, and the chips were heated to ~130°C. The reverse-proton-exchange waveguides were fabricated with our usual procedure.[2] The cross-correlation technique based on two-photon absorption[2,5] was chosen for Subsection 3.A to compare OPG in devices with different QPM grating lengths, while the frequency-resolved cross-correlation technique[3] was chosen for Subsection 3.B to thoroughly study cascaded OPG in a single waveguide device. The former used a GaAsP photodiode while the latter used a piece of $LiIO_3$ crystal and a silicon detector, with an experimental setup shown in Fig. 2. In this setup, by angle phase matching the type-I SFG between the signal (idler) and a reference beam split from the pump wave, the 0.25 mm thick $LiIO_3$ crystal served as a tunable bandpass filter with a filter function of $\mathrm{sinc}^2[(\lambda-\lambda_0)/\Delta\lambda]$. The bandwidth $\Delta\lambda$ of the filter was ~38 nm for the signal near 1430 nm. The center wavelength λ_0 was determined by the tilting angle of the $LiIO_3$ crystal. Using this filter, we can obtain the pulse shape in selected spectral ranges.[3]

A. Cascaded Optical Parametric Generation in Uniform Quasi-Phase-Matching Gratings of Different Lengths

Figure 3 shows the power spectra and the pulse shapes of the OPG signal from waveguides with uniform QPM grat-

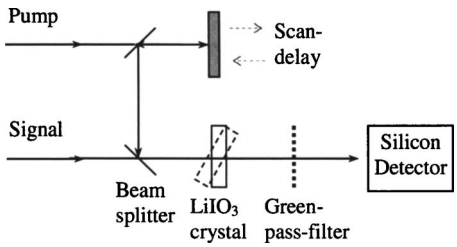

Fig. 2. Diagram of the frequency-resolved cross correlator. The scan delay ensures that the pump and signal pulses temporally overlap in the $LiIO_3$ crystal. By replacing the $LiIO_3$ crystal and the silicon detector with a GaAsP photodiode, we obtain a cross correlator without frequency resolvability.

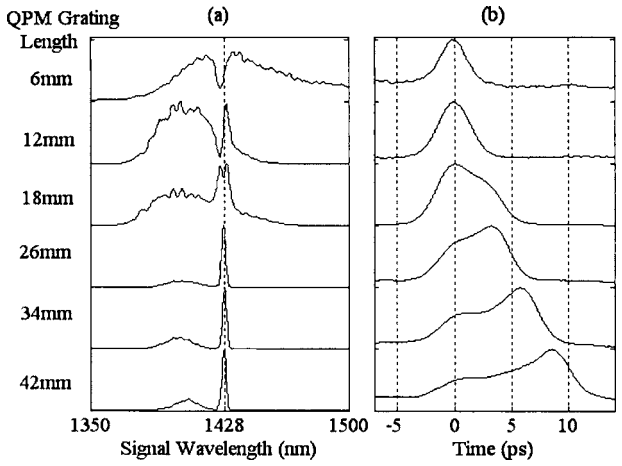

Fig. 3. (a) Power spectra and (b) the pulse shape for the signal from optical parametric generation in lithium niobate waveguides with different QPM grating lengths. The photon conversion efficiencies for all these traces were ~10% except for the 6 mm long gratings for which it was only 2%. The peak of the conventional OPG products is set as the time zero for all the curves in (b). All the curves are normalized to their maxima.

ings of different lengths. All the different devices were fabricated side by side on the same chip and the duty cycles of the QPM gratings were nominally 50%. The OPG threshold was ~200 pJ for the devices with QPM gratings longer than 18 mm, the same as observed in the previous measurements.[2] For a fair comparison, the pulse shape and spectra data were taken for the different grating lengths at pump powers resulting in total photon conversion efficiencies of ~10%, except for the 6 mm long gratings, which had only 2% efficiency with the maximum available pump power. This exception did not affect our conclusions because cascaded OPG output was absent in the 6 mm long QPM gratings.

The pulse shapes were obtained from cross-correlation measurements based on two-photon absorption in GaAsP photodiodes with a reference beam split from the pump.[2,5] In such a measurement, the signal and the idler outputs in the whole frequency range would be simultaneously recorded. Although the idler wave was not removed by a filter, according to simulations, it would only slightly affect the pulse shape recorded by cross correlation because the group velocity mismatch between the signal at ~1420 nm and the idler at ~1750 nm was $<\frac{1}{10}$ of that between the signal (idler) and the pump near 784 nm,[6] so that signal and idler pulses are nearly overlapping in time. We will experimentally verify this conclusion in Subsection 3.D after we have discussed the details of cascaded OPG in Subsections 3.B and 3.C.

By comparing curves in Fig. 3 to simulations, we can identify the conventional OPG and cascaded OPG products both in the frequency domain and in the time domain. In the frequency domain, the narrow peaks at ~1428 nm correspond to the cascaded OPG products. In the time domain, the time zero is set at the peaks of the conventional OPG products. Comparing the curves in Fig. 3, we can see how cascaded OPG and conventional OPG compete with each other. Only for gratings longer than 18 mm does the extra signal peak from cascaded OPG dominate in the frequency domain and become distinguishable in the time domain. The power spectra of the signal from QPM gratings shorter than 18 mm show strong interferences between the two different processes. When we isolated the cascaded OPG signal at ~1428 nm from the conventional OPG signal in the time domain by deconvolving the cross-correlation traces for the long gratings, a time-bandwidth product close to 0.4 was obtained for the cascaded OPG signal. These results complement those we obtained in Ref. 2, where we analyzed the evolution of the pulse shapes in a single device with an 18 mm long QPM grating at various pump power levels.

B. Identifying Cascaded Optical Parametric Generation and Conventional Optical Parametric Generation Products Using Frequency-Resolved Cross Correlation

In Subsection 3.A, we found the correspondence between the signal peaks in the time domain and the frequency domain and identified the conventional OPG and cascaded OPG peaks by measuring devices of different lengths. However, we can directly identify cascaded OPG and conventional OPG products by frequency-resolved cross-correlation measurements of a single waveguide at a fixed pump power, using the setup shown in Fig. 2. In such measurements, the ratio between the two peaks on the cross-correlation traces varies when the center of the filtering wavelength range is tuned. From this variation, we can identify which peak corresponds to cascaded OPG.

Figure 4 shows the power spectrum and the pulse shape for the signal from a device with a 34 mm long QPM grating at a pump power level resulting in a photon conversion efficiency of ~10%. Each curve in Fig. 4(b) is a frequency-resolved cross-correlation trace, corresponding to a wavelength range whose center wavelength is determined by the bandpass filter. This center wavelength is indicated by the baseline of the curve and can be read out from the x axis of Fig. 4(a). From the peak-intensity variations in the different curves in Fig. 4(b), we can deduce the correspondence between the two peaks in the frequency domain and the two sets of peaks in the time domain. The conventional OPG products and the cascaded

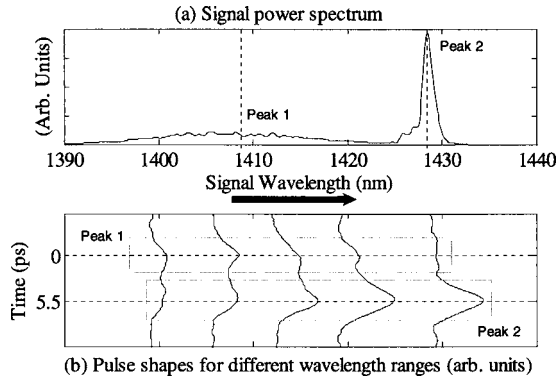

Fig. 4. (a) Signal power spectrum with a pump wavelength of 784.4 nm and a photon conversion efficiency of ~10%. (b) Pulse shapes of the OPG signal in different wavelength ranges with a 38 nm wide sinc^2-shape bandpass filter. To show the correct relative power the curves in (b) are not normalized. Baselines are shifted to indicate center signal wavelength for each trace, which can be read out from the x axis of (a). On each curve, peak 1 corresponds to the conventional OPG products, and peak 2 corresponds to the cascaded OPG products.

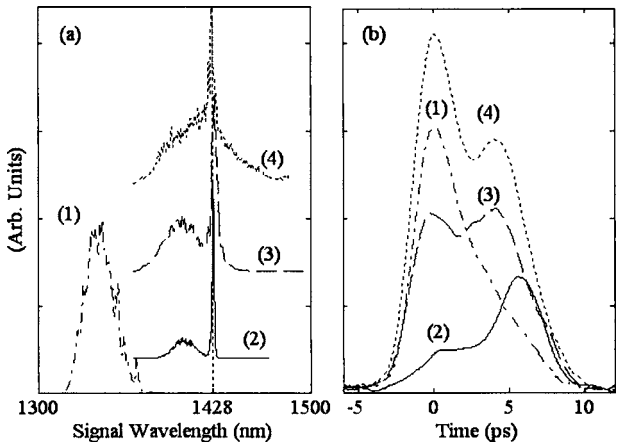

Fig. 5. (a) Signal power spectra and (b) the pulse shape for a waveguide with a 34 mm long QPM grating. In both figures, the dashed–dotted curves (1) correspond to a pump wavelength of 782.8 nm and a photon conversion efficiency of ~20%; cascaded OPG was absent. For the solid (2), dashed (3), and dotted (4) curves, the pump wavelength was 784.4 nm, strong cascaded OPG was present, and they, respectively, correspond to a total photon conversion efficiency of ~10%, 20%, and 30%. All the curves in (a) are normalized to their maxima and the baselines are shifted for a clear comparison in their peak positions, while the curves in (b) are not normalized and hence show a correct comparison in photon conversion efficiencies.

OPG products are, respectively, marked as peak 1 and peak 2. Although the large bandwidth of the thin $LiIO_3$ crystal used in the frequency-resolved cross correlation limited the contrast between the peaks on different curves in Fig. 4(b), the cascaded OPG and conventional OPG products are nevertheless identified and are consistent with results discussed in Subsection 3.A.

C. Analysis of Cascaded Optical Parametric Generation and Conventional Optical Parametric Generation under Different Levels of Pump Depletion

By summing up the frequency-resolved cross-correlation traces in different wavelength ranges, we can restore the pulse shape for the whole signal band with the idler contribution removed. Figure 5 shows the power spectra and the pulse shapes under different levels of pump depletion obtained in this way for the device used for Fig. 4. The dashed–dotted curves were obtained at a pump power level resulting in a photon conversion efficiency of ~20% when the pump wavelength was 782.8 nm and cascaded OPG was absent. All the other curves in Fig. 5 were obtained when the pump wavelength was 784.4 nm and the cascaded OPG signal was near 1428 nm. The photon conversion efficiency was, respectively, ~10%, 20%, and 30% for the solid, dashed, and dotted curves.

The experimental results match the simulation results obtained from solving Eq. 1 in Ref. 2, and for clarity are not shown on the figure. We can explain the different pulse shapes in Fig. 5(b) with the mechanisms of conventional OPG and cascaded OPG.

The dashed–dotted curve in Fig. 5(b) corresponds to conventional OPG with no cascading. Because the grating length of 34 mm was much longer than the walkoff length of ~5 mm between the signal and the pump, the output signal pulse would have a flat-top shape due to group-velocity mismatch if the pump is lossless, which is illustrated in Fig. 6. However, the propagation loss for the pump was ~0.3 dB/cm in the waveguides, and the pump depletion was significant when the photon conversion efficiency was 20%, and the gain depends exponentially on the pump power, so that most of the conventional OPG signal photons are generated in the front part of the QPM grating. The signal pulse shape thus became very asymmetric.

The solid, dashed, and dotted curves in Fig. 5 correspond to cascaded OPG and conventional OPG under different levels of pump depletion and can be explained by further considering the mechanism of cascaded OPG, which involves SFG and its backconversion.

In pure SFG, the power distribution among the interacting waves oscillates following $\sin^2(\sqrt{\eta_{SFG}P}L) = \sin^2[\pi L/(2L_0)]$ (Ref. 7) where η is the normalized gain parameter in the SFG and P is the peak pump power. L_0 is half the oscillation period, after which the backconversion of SFG starts if there is no input sum-frequency wave. Although the SFG in cascaded OPG is more complex than pure SFG, it still has a characteristic length for which we keep the notation L_0. As illustrated in Fig. 6, only after this length does the backconversion of SFG start and does cascaded OPG occur. The cascaded OPG signal photons therefore are generated in the rear part of the QPM gratings. The threshold of cascaded OPG is slightly higher than that of conventional OPG because the SFG is required. We can deduce from Fig. 3 that L_0 is ~12 mm, which is longer than the rough estimation of $L_0 \sim (\pi/2)/\sqrt{\eta_{SFG}P} = 5$ mm from $\eta_{SFG} = 10\%/\mathrm{W\,cm^2}$ at a peak pump power of 100 W. This discrepancy comes from the group-velocity walkoff neglected in the estimation. By numerically solving Eq. (1) in Ref. 2 we obtained the same value as the experimental result. Because the QPM grating length of 34 mm in the experiments was longer than L_0, cascaded OPG and conventional OPG coexisted.

For the solid curve in Fig. 5(b), the pump power was slightly higher than the OPG threshold. The exponential growth of cascaded OPG is much faster than that of conventional OPG because of the apparent group-velocity matching[8,9] between the signal (idler) and the pump. More photons therefore came from cascaded OPG than conventional OPG, and the portion of signal photons coming from cascaded OPG was 85% and was the major output. For the dashed and dotted curves in Fig. 5(b), the pump power was even higher. With stronger backconversion in cascaded OPG both the bandwidth and the pulse

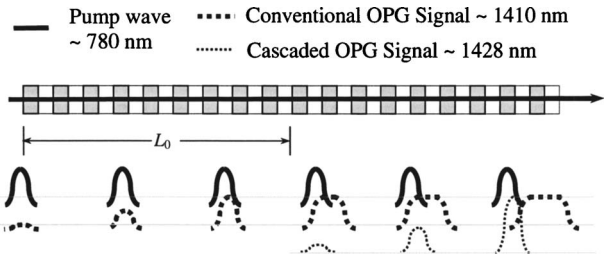

Fig. 6. Illustration of the different properties of conventional OPG and cascaded OPG. No propagation loss is considered for the pump. L_0 is the characteristic length for the SFG in cascaded OPG.

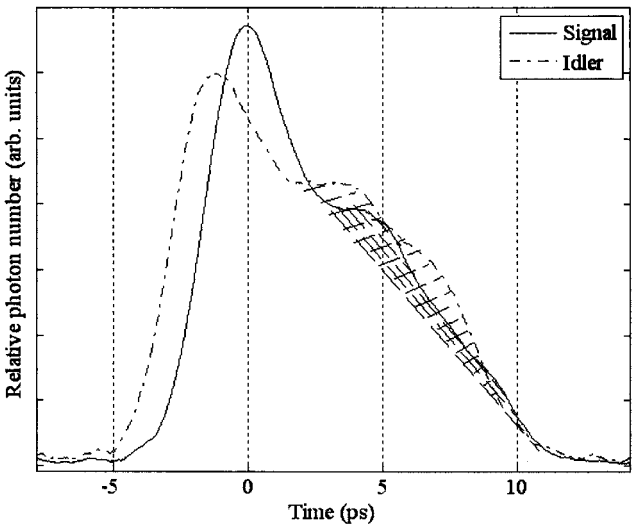

Fig. 7. Pulse shapes of the signal and idler obtained by summing up the frequency-resolved cross correlation traces from a 42 mm long QPM grating at a pump power resulting in a photon conversion efficiency of ~20%. The shadowed regions under the curves correspond to the cascaded OPG products while the other regions correspond to the conventional OPG products.

length of the cascaded OPG signal increased while the photon conversion efficiency no longer increased. However, more pump photons converted into signal and idler photons in the front part of the QPM gratings via conventional OPG, we thus obtained the pulse shapes shown by the dashed and dotted curves in which conventional OPG dominated.

D. Comparing the Shapes of the Signal and Idler Pulses from Optical Parametric Generation

Subsection 3.A, we declared that we can obtain the approximate pulse shape for the signal without removing the idler. Here we experimentally verify it by comparing the solid curve in Fig. 5(b) to the solid curve on the fifth row (from top) in Fig. 3(b), which correspond to the same QPM grating length of 34 mm and the same photon conversion efficiency of ~10%. Although both the signal and the idler were measured in the case of Fig. 3(b) while only the signal was measured by the method used in the case of Fig. 5(b), the pulse shapes observed for the output were similar, confirming that the presence of the idler does not significantly affect the pulse shapes measured without frequency resolving the cross correlation.

For a detailed comparison, we show the signal and idler pulse shapes in Fig. 7, obtained by summing up the frequency-resolved cross-correlation traces for the signal and the idler from a device with a QPM grating length of 42 mm at a pump power level resulting in a photon conversion efficiency of ~20%. The two curves in Fig. 7 were calibrated for the efficiencies of the SFG in the $LiIO_3$ crystal at the signal (idler) wavelengths. The peak positions in the two traces are different because the group velocity of the idler at ~1.8 μm is slightly faster than that of the signal near 1.4 μm. In contrast to the signal pulses from a 34 mm long QPM grating shown in Fig. 5, the signal and idler pulses for the 42 mm long QPM grating in Fig. 7 have three peaks. We obtained this complex pulse shape because the grating length (42 mm) was over three times of the characteristic length (~12 mm) of the SFG in cascaded OPG [see Subsection 3.C for details]. We had obtained a square pulse shape at a lower pump power level in the former experiments[2] because the pulse length of the pump in the cross correlation was comparable to the time interval between the three peaks, smearing out the cross correlation. The optimized grating length is therefore ~34 mm to obtain cascaded OPG signals with the best temporal properties.

4. EXPERIMENTS WITH ENGINEERED QUASI-PHASE-MATCHING GRATINGS

To explore wideband tuning of the transform-limited signal from cascaded OPG, which is distinguishable from a background of conventional OPG signal, we designed devices to generate various signal wavelengths from cascaded OPG.

As we discussed in Section 2, cascaded OPG was weakly dependent on the pump wavelength or temperature so that the signal wavelength tuning range was only several nanometers in uniform QPM gratings. Tuning over a broad range of signal wavelengths requires another method for controlling cascaded OPG. Devices with QPM gratings having the same QPM period Λ_{OPG} for OPG and different QPM periods Λ_{SFG} for SFG allow such control.

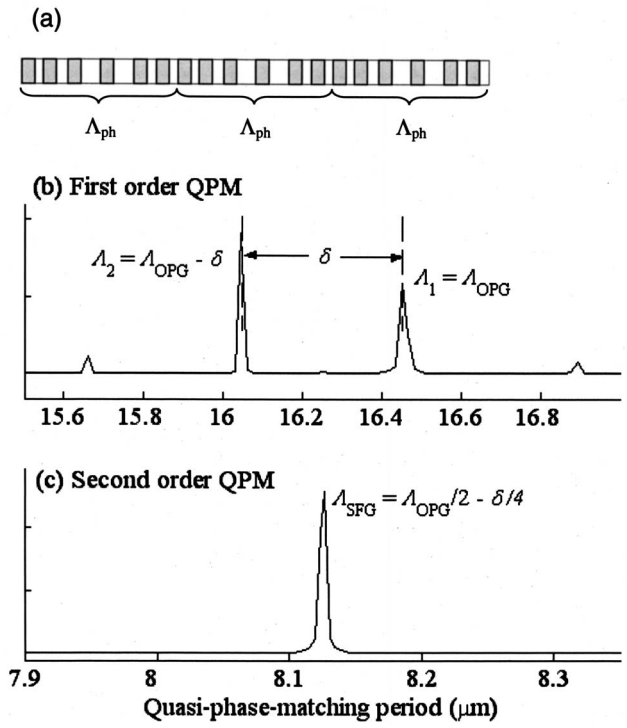

Fig. 8. (a) Diagram of the phase-modulated gratings. The center positions of the domains shift by an amount calculated from an optimized periodic phase function. Λ_{ph} is the phase-modulation period. (b), (c) Simulated QPM peaks of phase-reversal gratings designed with $\Lambda_1=\Lambda_{OPG}=16.45$ μm, $\delta=0.4$ μm, and $\Lambda_2=\Lambda_1-\delta=16.05$ μm (see text for definition of symbols). The grating duty cycle is $\frac{1}{3}$ and the two peaks near Λ_1 and Λ_2 have the same area in the spatial-frequency domain.

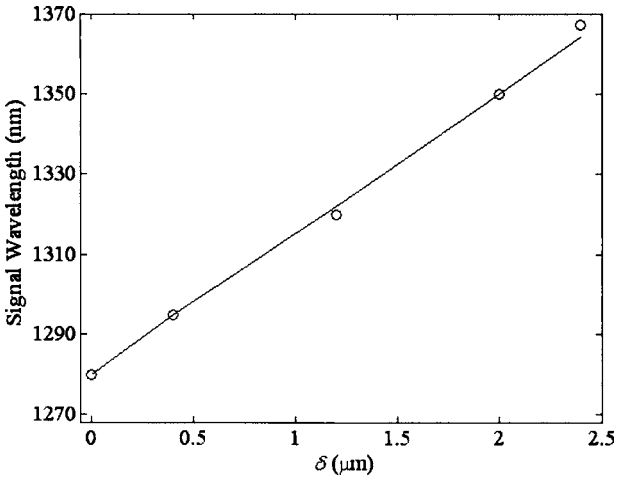

Fig. 9. Wavelengths of the signal from the strongest cascaded OPG in different phase-modulated gratings. δ is a parameter describing the QPM grating design, defined in the text and shown in Fig. 8. The solid line is from simulations without any adjustable parameter, and the circle symbols are from experimental results.

Although several approaches[10–13] exist for engineering such multicomponent gratings, for demonstration we choose phase-modulated gratings for their loosest fabrication tolerances. In periodically poled lithium niobate, the phase modulation is realized with a poling mask, which periodically shifts the center positions of the domains with a period Λ_{ph}, which is illustrated in Fig. 8(a). The shifting function is obtained by numerical optimizations to have quasi-phase-matching peaks with desired positions and amplitudes in the Fourier spectrum.[10]

To understand the properties of phase-modulated gratings, we study phase-reversal gratings,[11] the simplest phase-modulated gratings with a QPM period Λ and a 50% duty cycle of phase reversal. These gratings have two first-order QPM peaks of the same amplitude close to each other in the Fourier spectrum at $\Lambda_1=\Lambda+\delta/2$ and $\Lambda_2=\Lambda-\delta/2$ where $\delta=2\Lambda^2/\Lambda_{ph}\ll\Lambda$. When the domain duty cycle is 50%, there is no second-order peak and only two third-order QPM peaks at $\Lambda_1/3$ and $\Lambda_2/3$. When the domain duty cycle is $\frac{1}{3}$ there is only one second-order QPM peak at $\Lambda_{SFG}=\Lambda/2$ and no third-order QPM peak, which is shown in Figs. 8(b) and 8(c). If we want different amplitudes for the two first-order QPM peaks at Λ_1 and Λ_2, we can no longer use phase-reversal gratings, so we designed phase-modulated gratings with the method described in Ref. 10. The general features of higher-order QPM peaks for such phase-modulated gratings are similar to those of the phase-reversal gratings but offer more degrees of freedom to tailor details of the Fourier spectrum.

To reduce the complexity, we prefer phase-modulated gratings with a domain duty cycle of $\sim\frac{1}{3}$, using the first-order QPM peak at $\Lambda_1=\Lambda_{OPG}$ for OPG and the highest second-order QPM peak at $\Lambda_{SFG}=\Lambda/2=\Lambda_{OPG}/2-\delta/4$ for the SFG. In the devices fabricated, $\Lambda_{OPG}=16.45$ μm and the nominal domain duty cycles were $\sim$40% in the 18 mm long QPM gratings while δ varied. To keep a low OPG threshold, the designed gain ratio between the two peaks at Λ_1 and Λ_2 was 7:3 so that the normalized gain parameter η for OPG would be 70% of that in a uniform QPM grating. Both in simulations and in second-harmonic generation measurements, the sum of η at the two peaks Λ_1 and Λ_2 was $>$90% of η in a uniform QPM grating, and the peak ratio was close to the designed value 7:3. For these parameters, a series of second- or third-order QPM peaks exist while the one at Λ_{SFG} is the largest. Figure 9 shows that the measured wavelengths of the signal from the strongest cascaded OPG match well with the simulations and vary almost linearly with δ in the signal wavelength range from 1280 to 1370 nm. The simulations were based on the waveguide dispersion from a model of reverse-proton-exchange lithium niobate waveguides without any adjustable parameter.[14] Similar to the results from uniform gratings, the signal peaks at these wavelengths had narrow bandwidths, indicating that near-transform-limit signal pulses were obtained. Although for $\delta\neq 0$, a weak signal from cascaded OPG appeared at approximately 1280 nm, which corresponded to the second strongest second-order QPM peak, we can design more sophisticated QPM gratings to avoid this problem, though these require precise control of the waveguide uniformity and QPM grating duty cycles and await future experiments.[15]

5. SUMMARY

Similar to conventional OPG, two problems limit practical applications of cascaded OPG in reverse-proton-exchange congruent lithium niobate waveguides. The most severe problem is photorefractive damage by the green and blue waves generated in the devices, even if we heat up the chips to 130°C. The blue waves come from parasitic second-harmonic generation of the pump and most of the green waves come from the SFG involved in cascaded OPG. Although the green wave from SFG is unavoidable in cascaded OPG and eliminating other parasitic products is difficult, this problem may be solved with new photorefractive-damage-resistant materials.[16–18] The second problem is the bottleneck in power conversion efficiency. Both cascaded OPG and conventional OPG have a bottleneck in conversion efficiency because only part of the leading edge of the pump pulse participates in the nonlinear interactions. An alternative to cascaded OPG is to compensate for the group-velocity mismatch between the signal (idler) and the pump with periodic waveguide structures so that the whole pump pulse may participate in the photon conversion.[19] Simulations and experimental results show that the signal generated in such a device also have well-controlled temporal properties.[20]

In summary, we systematically and experimentally studied cascaded optical parametric generation in reverse-proton-exchange waveguides in congruent lithium niobate with different QPM grating lengths. By using a frequency-resolved cross correlator, we characterized the temporal properties of the signal generated in cascaded OPG and studied the process in the regime of strong pump depletion. We also demonstrated control over the signal wavelength from cascaded OPG by using phase-modulated-QPM gratings. By switching between waveguides with different grating designs and fine tuning the pump wavelengths, obtaining transform-limited and wavelength-tunable signals from cascaded OPG is possible.

ACKNOWLEDGMENTS

This research was sponsored by the Air Force Office of Scientific Research under AFOSR grant F49620-02-1-0240. We acknowledge the support of Crystal Technology, Inc.

Xiuping Xie's e-mail address is xpxie@stanford.edu.

REFERENCES

1. A. Galvanauskas, M. A. Arbore, M. M. Fejer, M. E. Fermann, and D. Harter, "Fiber-laser-based femtosecond parametric generator in bulk periodically poled $LiNbO_3$," Opt. Lett. **22**, 105–107 (1997).
2. X. Xie, A. M. Schober, C. Langrock, R. V. Roussev, J. R. Kurz, and M. M. Fejer, "Picojoule threshold, picosecond optical parametric generation in reverse proton-exchanged lithium niobate waveguides," J. Opt. Soc. Am. B **21**, 1397–1402 (2004).
3. C. Radzewicz, P. Wasylczyk, and J. S. Krasinski, "A poor man's FROG," Opt. Commun. **186**, 329–333 (2000).
4. T. Südmeyer, F. Brunner, R. Paschotta, T. Usami, H. Ito, M. Nakamura, K. Kitamura, and U. Keller, "Femtosecond optical parametric generation (OPG) in periodically poled stoichiometric $LiTaO_3$ with >1 W average power," in *Conference on Lasers and Electro-Optics* (Optical Society of America, 2002), Paper CTuO4.
5. J. K. Ranka, L. Gaeta, A. Baltuska, M. S. Pshenichnikov, and D. A. Wiersma, "Autocorrelation measurement of 6-fs pulses based on the two-photon-induced photocurrent in a GaAsP photodiode," Opt. Lett. **22**, 1344–1346 (1997).
6. D. H. Jundt, "Temperature-dependent Sellmeier equation for the index of refraction, n_e, in congruent lithium niobate," Opt. Lett. **22**, 1553–1555 (1997).
7. R. W. Boyd, *Nonlinear Optics* (Academic, 1992).
8. A. V. Smith, "Group-velocity-matched three-wave mixing in birefringent crystals," Opt. Lett. **26**, 719–721 (2001).
9. P. D. Trapani, A. Andreoni, C. Solcia, P. Foggi, R. Danielius, A. Dubietis, and A. Piskarskas, "Matching of group velocities in three-wave parametric interaction with femtosecond pulses and application to traveling-wave generators," J. Opt. Soc. Am. B **12**, 2237–2244 (1995).
10. M. Asobe, O. Tadanaga, H. Miyazawa, Y. Nishida, and H. Suzuki, "Multiple quasi-phase-matched $LiNbO_3$ wavelength converter with a continuously phase-modulated domain structure," Opt. Lett. **28**, 558–560 (2003).
11. M. H. Chou, K. R. Parameswaran, and M. M. Fejer, "Multiple-channel wavelength conversion by use of engineered quasi-phase-matching structures in $LiNbO_3$ waveguides," Opt. Lett. **24**, 1157–1159 (1999).
12. T. Kartaloglu, Z. G. Figen, and O. Aytur, "Simultaneous phase matching of optical parametric oscillation and second-harmonic generation in aperiodically poled lithium niobate," J. Opt. Soc. Am. B **20**, 343–349 (2003).
13. H. Liu, Y. Y. Zhu, S. N. Zhu, C. Zhang, and N. B. Ming, "Aperiodic optical superlattices engineered for optical frequency conversion," Appl. Phys. Lett. **79**, 728–730 (2001).
14. R. Roussev, X. P. Xie, K. R. Parameswaran, M. M. Fejer, and J. Tian, "Accurate semiempirical model for annealed proton exchanged waveguides in z-cut lithium niobate," in *Lasers and Electro-Optics Society Meeting Proceedings* (IEEE, 2003), Paper TuS4.
15. J. Huang, X. P. Xie, C. Langrock, R. V. Roussev, D. S. Hum, and M. M. Fejer, "Amplitude modulation and apodization of quasi-phase-matched interactions," Opt. Lett. **31**, 604–606 (2006).
16. M. Asobe, H. Miyazawa, O. Tadanaga, Y. Nishida, and H. Suzuki, "A highly damage-resistant $Zn:LiNbO_3$ ridge waveguide and its application to a polarization-independent wavelength converter," IEEE J. Quantum Electron. **39**, 1327–1333 (2003).
17. M. Katz, R. K. Route, D. S. Hum, K. R. Parameswaran, G. D. Miller, and M. M. Fejer, "Vapor-transport equilibrated near-stoichiometric lithium tantalate for frequency-conversion applications," Opt. Lett. **29**, 1775–1777 (2004).
18. T. Sugita, K. Mizuuchi, K. Yamamoto, K. Fukuda, T. Kai, I. Nakayama, and K. Takahashi, "Highly efficient second-harmonic generation in direct-bonded $MgO:LiNbO_3$ pure crystal waveguide," Electron. Lett. **40**, 1359–1361 (2004).
19. J. Huang, J. R. Kurz, C. Langrock, A. M. Schober, and M. M. Fejer, "Quasi-group-velocity matching using integrated-optic structures," Opt. Lett. **29**, 2482–2484 (2004).
20. X. Xie, J. Huang, and M. M. Fejer, "Narrow-linewidth near-degenerate optical parametric generation achieved with quasi-group-velocity-matching in lithium niobate waveguides," Opt. Lett. **31**, 2190–2192 (2006).